Joining Retinal Vessel Segments

Bashir Al-Diri, Andrew Hunter, David Steel and Maged Habib

***Abstract*—A new method is introduced for joining vessel segments together to form a vessel graph. Using a reference image set from the Sunderland Eye Infirmary, we analysed the retinal bifurcation geometry, to define measurements for the geometrical junction features. These distinctive measurements are employed to resolve the junctions. Self organized feature maps (SOFM) are used to "learn" cost functions for forming bifurcation and bridge forms. The system joins segments depending on their "projective intersections" and the SOFM cost functions. The system includes algorithms to handle overlapping and parallel segments. Transferring the vascular network to a vascular graph provides an opportunity to extract more information and to calculate features that have been not previously calculated, by providing new measurements from graph theory.**

***Index Terms*—Parametric active contour, A self organized feature map, vascular network, vascular junction.**

I. Introduction

A number of authors have presented algorithms to detect retinal vascular networks, including [1], [2], [3], [4]. Usually these algorithms are less reliable in detecting junctions than vessels segments between junctions. This paper presents algorithms for the detection of vessel junctions, on the assumption that segments have been previously calculated.

An analysis of retinal vascular junctions is presented, and used to define a list of junction measurements that are employed in the junction resolution algorithm. The segments may be joined using one of three types of *joining forms*: *bifurcations*, *bridges* and *leaves* (unjoined). The *self organizing feature map* (SOFM) is trained using junction measurements to estimate the cost of a joining form given its feature measurements. The segment ends are gathered together in local sets under geometrical and functional conditions. In each set, the segment ends may join different joining forms, so that there are various possible configurations of joining forms – *cases*. The chosen case has the total cost over its joining forms.

II. Materials

A retinal image set, the *geometric image set* (GIS) is used to analyse the geometrical features of the retinal bifurcations, to guide the design of the joining algorithms. The GIS was selected from the fundus images database of the diabetic retinopathy clinic at Sunderland Eye Infirmary. Retinal photography was performed to all patients according to a standardised protocol as part of their routine clinical care. Mydriasis was induced using tropicamide (1%) eye drops. All images were independently graded by a qualified diabetic retinopathy grader adopting the modified classification developed for the EURODIAB IDDM complication study [5]. The GIS consists of 21 images; these images were graded as follows; 12 images are normal, one image is level one (Minimal Non-proliferative Retinopathy), three images are level two (Moderate Non-Proliferative Retinopathy), two images are level three (Severe Non-Proliferative Retinopathy) and three images are level five (Proliferative Retinopathy). There are 435 marked junctions. The main features of each junction have been measured: segment widths, segment directions and segment head intensities. Segments were categorized as *Arteries* and *Veins*.

A. Geometrical Features

The basic measurements associated with the bifurcations are shown in Figure 1. The use of actual measurements such as diameters is associated with difficulties and errors, particularly when the measurements are taken from a magnified images of the bifurcation. Theses problems can be avoided by specifying a bifurcation in terms of relatives, rather than actual, measurements. The angles θ, θ_1 and θ_2 are used to assess the branching geometry at a bifurcation; the diameter ratios $\alpha = d_2^2/d_1^2$, $\beta = (d_1^2 + d_2^2)/d_0^2$, $\lambda = d_2/d_1$, $\lambda_i = d_i/d_0$ and junction exponent(K): $d_0^K = d_1^K + d_2^K$ are used to assess the relation between segment diameters.

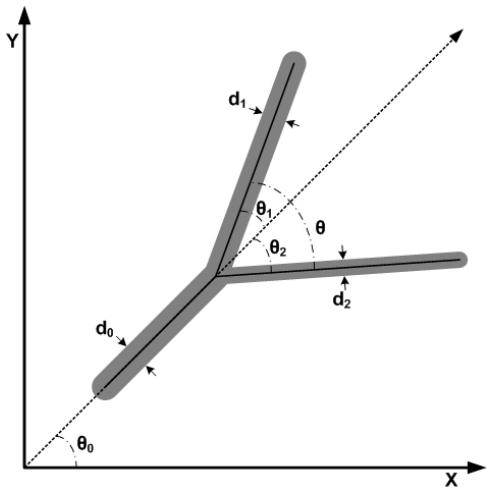

Fig. 1. The basic bifurcation features: diameters (d_i) and bifurcation angles (θ, θ_i).

The values of these features are described in Table I.

The analysis focusses mainly on three parameters: angles, widths and intensity.

Bashir Al-Diri is with the Department of Computing and Informatics, University of Lincoln, UK baldiri@lincoln.ac.uk

Andrew Hunter is the Dean of Research, University of Lincoln, UK ahunter@lincoln.ac.uk

David Steel is with Sunderland Eye Infirmary, a Consultant Ophthalmologist, UK

Maged Habib is with Sunderland Eye Infirmary, a Specialist Registrar in Ophthalmology, UK

	No	Min	Max	Mean	Std E	Std D	Var
d_0	435	4.67	19.78	9.47	0.13	2.69	7.23
d_1	435	3.78	17.51	8.36	0.12	2.49	6.18
d_2	435	1.06	12.91	6.36	0.08	1.74	3.01
α	435	0.01	1.32	0.64	0.01	0.23	0.06
β	435	0.66	1.86	1.27	0.01	0.22	0.05
λ	435	0.11	1.15	0.79	0.01	0.16	0.03
λ_1	435	0.61	1.05	0.88	0.00	0.08	0.01
λ_2	435	0.11	0.97	0.69	0.01	0.13	0.02
K	435	0.00	27.13	3.96	0.13	2.71	7.32
θ	435	43.75	132.32	80.17	0.70	14.62	213.87
θ_1	435	-18.09	70.21	23.23	0.65	13.47	181.45
θ_2	435	10.17	97.72	56.94	0.77	16.14	260.44

TABLE I
DESCRIPTIVE STATISTICS OF RETINAL JUNCTION FEATURES: THE PARENT WIDTH (d_0), FIRST CHILD SEGMENT WIDTH (d_1), SECOND CHILD SEGMENT WIDTH (d_2), ASYMMETRIC RATIO (α), AREA RATIO (β), BIFURCATION INDEX (λ), FIRST DIAMETER RATIO (λ_1), SECOND DIAMETER RATIO (λ_2), JUNCTION EXPONENT (K), BIFURCATION ANGLE (θ) AND BRANCH ANGLES (θ_1, θ_2).

III. JOINING UP THE VASCULAR NETWORK

The algorithm is initialised with a set of vessel segments extracted in a previous processing stage; we use the "Ribbon of Twins" [6] algorithm, which gives reliable results; see Figure 2.

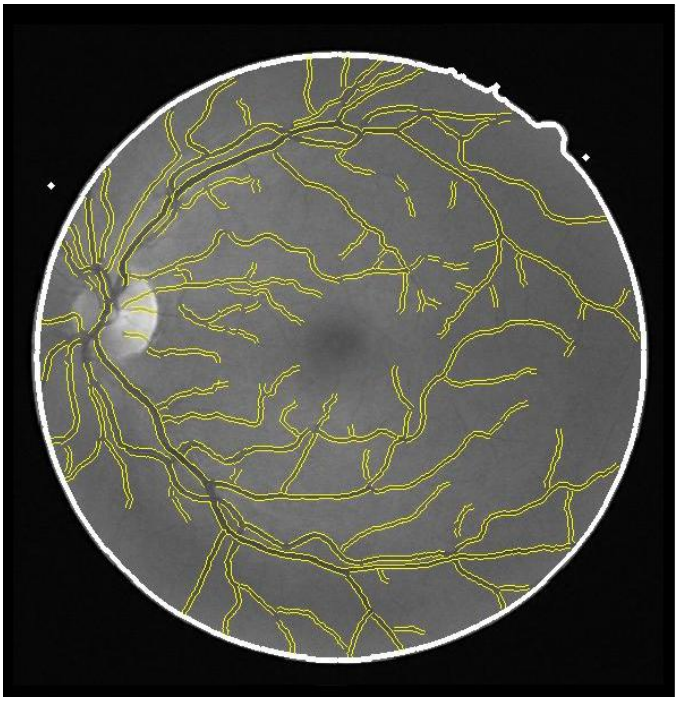

Fig. 2. The extracted segments of the first image from test set of the DRIVE database [7].

A. Segments

Segments of different types: veins and arteries, do not connect with each other directly, although they may cross each other. Each segment in the vascular retinal network has two ends: the head and the tail. The segment ends are classified into three types: *leaf segment ends*, where segment ends are inside the macula, reach the image rim or have no other segment ends nearby; *root segment ends*, where segment ends are located inside the optic nerve head (ONH); root segment ends are not covered further in this work; and *joinable segment ends*; see Figure 3.

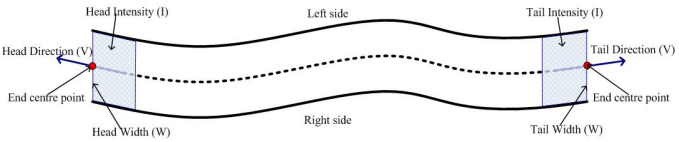

Fig. 3. Segment end profiles contain end centre point, local direction, width and intensity.

The three types of segment ends are differentiated by assessing their neighbouring segment ends. It is worth noting that the nearest neighbouring segment ends do not always form a junction, and they sometimes lie some distance away from the correct joining position. Gaps appear between segments either because of normal features such as junctions, crossings and overlays, or because of abnormal features such as pathology, noisy and corrupted edges and very low contrast. It can be particularly hard to detect the vessel edges (which are often traced by robust segmentation algorithms); however, the vessel ridge is almost still visible and can be traced.

B. Centre Line Growing

The centre line of the vessel is located on the vessel ridge. The centre lines are grown using a twin contours as defined in ROT [6]. The segment centre line is grown iteratively using the twin; on each iteration the stopping conditions below (which identify the segment end type) are tested.

1) *Leaf*,
   a) if the growing centre point reaches the image rim,
   b) if the growing centre point reaches the Macula rim (if Macula is defined),
   c) if there is no segment end within radius equal half the ONH radius,
   d) if the growing centre line is longer than half the ONH radius.
2) *Root*, if the growing centre point reaches or falls inside the ONH (this does not occur in our research).
3) *Joinable*, if the nearest segment end is less than the width of the growing segment end.

The algorithm continues until all the segment ends are categorized as leaf or joinable.

C. Creating local sets

Joining between segment ends has three forms: first, the *leaf form*, where the segment end is not joined to any other segment ends; second, the *bridge form*, which joins two sub-segments to fill a gap between them; third, the *junction form*, which joins three segment ends forming a bifurcation. These joining forms represent all acceptable junctions that might occur in the retinal network. The term *local set* is used to represent a group of segment ends within a vicinity that might conceivably join each other. Each segment end belongs to a single local set. During set assignment, we first check each

segment end for "projective intersection" with the segment ends nearest to it. When projective intersections occur, the two segments are assigned to the same set, creating new sets, joining existing one or merging existing ones as necessary. Having completed this stage, we repeat for all unresolved segment ends using the next nearest neighbors, then with the second nearest neighbours (three levels of neighbours have proved sufficient in all our experiments).

1) Projective Intersection Algorithm: To assign segment ends to local sets, we use a "projective intersection" algorithm. Given two segment ends, we project the centre lines and edge lines of each, detecting intersection of the two centre lines, and intersection of any of the three lines with the line segment joining the two end points of the other segment's edges; see Figure 4. The total of seven possible collisions defines a measure, the *collision score* ($c_{ij} = N/7$), where N is the number of collisions that occur.

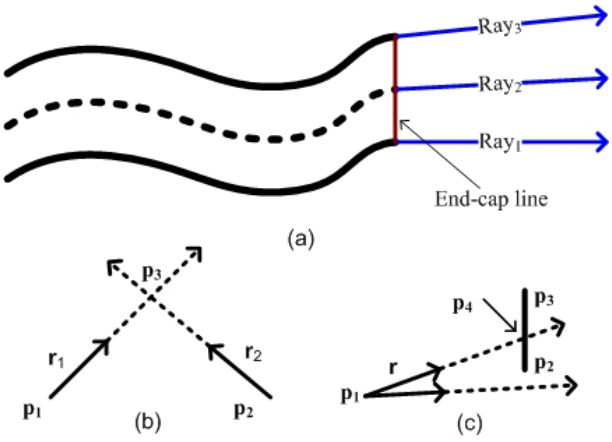

Fig. 4. An illustration of segment end intersections. (a) The segment end represented as three rays and an end-cap line. (b An intersection between two rays. (c) An intersection between ray and end-cap line.

D. Features of Joining Forms

The cost function parameters are defined according to features of the topology and geometry of the joining form. Two questions arise at this stage: given three segment ends what is the likelihood that they form a valid bifurcation; given two segment ends, what is the likelihood that they form a valid bridge? We base the decision on appropriate feature vectors. The vector of bifurcation geometric features (BfGF) consists of α, β, λ, λ_1, λ_2, θ, θ_1, θ_2, which are described in section II-A; the vector of bridge geometric features (BgGF) of $(\lambda_1, \varphi, \eta)$ (defined below). Defining ρ_i as the mean intensity of the i^{th} segment end (of pixels within the last three profiles), and $\mathbf{v_i}$ as the segment direction vector, the parameters are defined as:

$$\lambda_1 = \frac{min(d_1, d_2)}{max(d_1, d_2)}. \quad (1)$$

$$\varphi = \frac{\arccos(\mathbf{v_1}.\mathbf{v_2})}{\pi} \quad (2)$$

$$\eta = \frac{min(\rho_1, \rho_2)}{max(\rho_1, \rho_2)}, \quad (3)$$

From a study of the GIS, the parent and the first child segments are used to simulate two subsegments separated by a gap. The discrepancies between the parent and the first child segments should be higher than that between two consecutive subsegments. Therefore, the discrepancy features between their width, their intensity and their direction are extracted. Table II shows the descriptive statistic of the BgGF vector.

	No	Min	Max	Mean	Std E	Std D	Var
λ_1	430	0.61	1.00	0.88	0.004	0.074	0.005
φ	430	0.68	1.00	0.88	0.003	0.063	0.004
η	430	0.80	1.00	0.96	0.002	0.033	0.001

TABLE II
DESCRIPTIVE STATISTICS OF THE BRIDGE GEOMETRIC FEATURES (BGGF) IN THE GIS.

The relationship between the parameters in these joining forms is complex, making it difficult to model a cost function explicitly. Instead, we define an *implicit cost function* by training a self organizing feature map (SOFM) [8], which is an unsupervised artificial neural network model. This consists of neurons organized on a regular low-dimensional grid, called the map. During learning, the SOFM develops "prototype vectors" on the neurons, which represent typical values of the input vector; during execution, the output of the SOFM is the Euclidean distance of the input vector from the nearest prototype vector. The SOFM is trained using a set of typical input vectors (in our case, taken from the GIS). The output of the SOFM is a *novelty* signal – zero for a perfectly recognised input, and progressively higher for less familiar inputs. It may thus be treated as a cost function, with unfamiliar configurations of junctions parameters being assigned a high cost.

Two SOFMs are created, the J_{sofm} and the B_{sofm}, each with topological map dimensions 8×6 nodes.

E. Cases of Joining Forms

Once the local sets are created, we can resolve each independently. A set of joining forms that could be generated from a local set is called a *case*. We consider all possible configurations of joining forms in the set, and choose the best configuration by sum of the joining form costs.

1) Cost of Bifurcation Form: The bifurcation cost (J_{cost}) is the product of the *intersection cost* $(1 - C_{12}C_{23}C_{31})$ which depends on the likelihood of collision between segment ends and the *optimum cost* (J_{sofm}), which provided by a SOFM. So $J_{cost} = J_{sofm}(1 - C_{12}C_{23}C_{31})$.
2) Cost of Bridge Form: The bridge cost (B_{cost}) is the product of the *intersection cost* $(1 - C_{12})$ and the *optimum cost* (B_{sofm}). So $B_{cost} = B_{sofm}(1 - C_{12})$.
3) Cost of Leaf Form: We define the cost of a leaf as the "opportunity cost" of not connecting it to the best available bridge or bifurcation; that is, the cost is unity minus the minimum cost of all possible joining forms that include the leaf. This ensures that the system penalizes the assignment of segment ends to leaves that can form high likelihood junctions or bridges.

F. Overlapping Segments

Segments of different types may cross each other at different angles. When the crossing angle is small, the crossing area length increases. When the crossing area length becomes longer than the diameters of the segments, the crossing area is called an *overlapping* area or *overlapping segment*, where parts of segment are hidden beneath the other one; see Figure 5. Figure 6 shows different type of overlap examples. The first

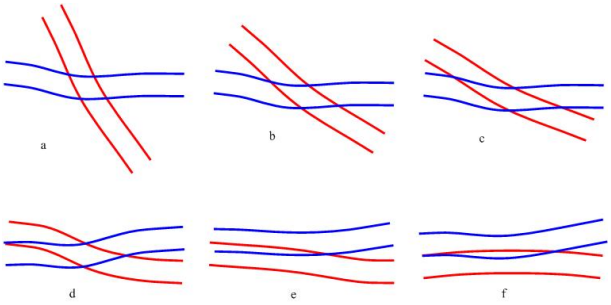

Fig. 5. An illustration shows two segments at different positions forming overlaps

row shows segments crossing each other, and the second row shows an example of the second type where a junction is formed when these segments meet each other in a crossing as in Figure (d); or a non-crossing as in Figure (e) and (f).

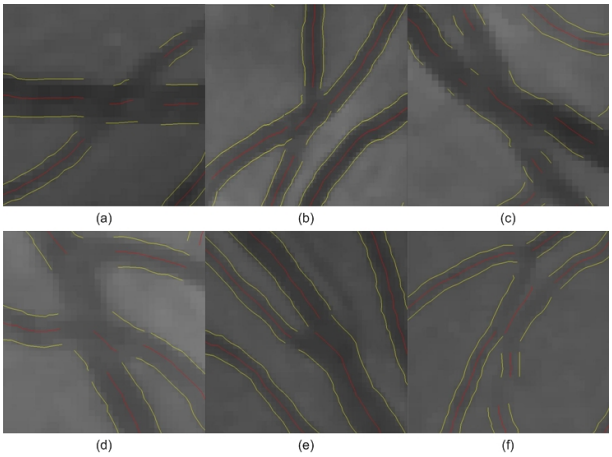

Fig. 6. Examples of different types of overlap segments. The first row shows different examples for overlapping segments of the first type. The second row shows examples of the second type; (d) an overlapping segment part before a crossing part; Figures (e) and (f) are an examples of two overlapping segments without crossing (closely parallel segments).

1) Overlapping Segment Detection: Two types of overlapping segments can be recognized. Figure 5 (a-c), shows an overlapping segment that is about to become a parent segment to two junctions. The other type of overlapping segment is illustrated in Figure 5 (d-f), where the overlapping segment is almost the parent segment of one junction. Figure 5 (e-f) shows the first part of the overlapping segments before the crossing starts, where the two segments are closely parallel; their segments may form a crossing or may not. The overlapping segment detecting algorithm considers sets with three members. For the first type of overlapping segment, segments that belong to two sets are collected. These may be overlapping segments if:

- The segment length is less than half of the ONH radius.
- The segment width is wider than that of the child segments.
- The segment ends at each junction are very close to each other; thus, the distance between segment ends is less than double the summation of segment widths.
- The segment is parent segment to two junctions at both ends. The segments of both set, at the both ends, have two sequences to form junctions, because the parent segment is not swapped. These sequences are assessed using the cost of the bifurcation form algorithm. The successful sequence with minimum cost represent a junction at each set.
- The θ angles of both junctions are less than the mean of the θ angles (80.17^o) of the bifurcations as reported in Table I.

The second type of overlapping segment, where the overlap segment is a parent segment to a single junction, is detected if:

- The segment length is less than half of the ONH radius.
- The segment width is wider than that of the child segments.
- The distance between segment ends is less than double the summation of the segment widths.
- The segment successfully forms a junction with and is identified as the parent segment.
- The θ angle is less than the minimum θ angles (43.75^o) of bifurcations as reported in Table I.

2) Extracting Segments from Overlapping Segments: In the first type, the overlapping segment is replaced by two bridge segments. Each face to face segment end connects to the other using a bridge. The cost of the bridge form algorithm is employed to explore the viability of connecting face to face segment ends. If the cost is below a threshold for both bridges, then bridge segments are created to connect face to face segment ends. The first row of Figure 7 shows the extracted bridge segments. For the second type, the overlapping segment is divided into two segments corresponding to the other two segment widths. Each edge of the overlapping segment corresponds to one of the involved segments. The second (internal) edge is defined related to its segment width; see second row of Figure 7.

IV. Results

The performance of the overlapping segment detection algorithm is assessed using the first five images of the DRIVE database. There are 27 overlapping segments. The algorithm detects 21 overlapping segments, including one false positive, thus the sensitivity and precision of the algorithm are 74% and 95% respectively. From the correct overlapping segments, 33% and 67% of detected overlapping segments are from the first and second types respectively. The false positive is of the second type. The undetected cases are more complex cases where the overlapping segments are long and some

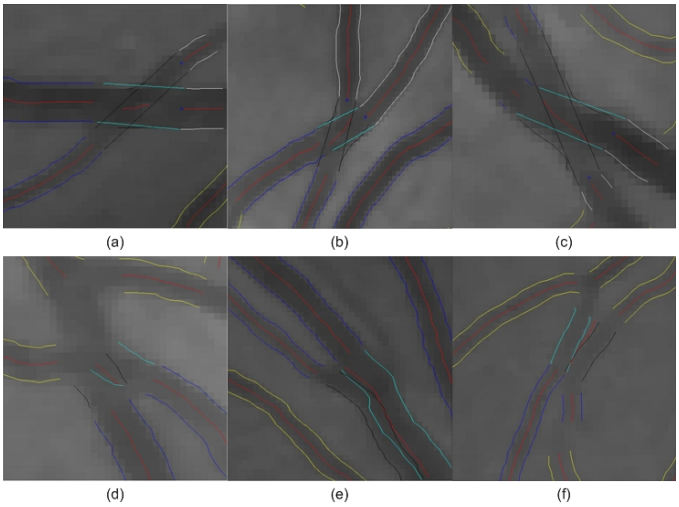

Fig. 7. The proposed solutions for junctions in Figure 6.

parts are not extracted; in addition, some bifurcate during the overlapping.

The performance of the segment joining and graph forming algorithm is assessed using the first five images from the DRIVE database. Table III shows the performance for each joining form. The true positive rate (TP), false positive rate (FP) and precision, which is the proportion of positive cases of positively classified cases, are defined.

Image	Detected Bifurcation			Detected Bridge			Detected Leaf		
	No	FP	Precision	No	FP	Precision	No	FP	Precision
1	59	7	89%	118	8	94%	22	2	92%
2	41	5	89%	56	3	95%	2	1	67%
3	56	6	90%	95	3	97%	7	1	88%
4	39	7	85%	55	2	96%	15	2	88%
5	56	5	92%	91	4	96%	14	1	93%

TABLE III
THE PERFORMANCE ON EACH JOINING FORMS ARE MEASURED USING THE FIRST FIVE DRIVE IMAGES.

Over the five images, 281 junction joining forms, 435 bridge joining forms and 67 leaf joining forms are detected; see Table IV.

Joining forms	TP	FP	Precision
Bifurcation form	251	30	89%
Bridge form	415	20	95%
Leaf form	60	7	90%

TABLE IV
THE PERFORMANCE OF THE JOINING FORMS CALCULATED USING THE FIRST FIVE IMAGES FROM THE DRIVE DATABASE.

The retinal vascular network is transfered to a vascular graph, represented by nodes (joining forms) and edges (segments). The vascular graphs are illustrated overlaid on their retinal images; see Figure 8.

V. CONCLUSION

The physiological constraints underlying the formation of vascular junctions are still not fully understood, requiring more mathematical analysis. We analyzed a reference data set to define measurements of the geometrical features of retinal bifurcations. These distinctive measurements were employed to build an algorithm for joining vessel segments. The system requires a cost function, to allow the selection of viable vascular junctions. Since an analytical form for this cost function is not available, we employed SOFM neural networks to estimate the cost function from data. These were trained from the GIS data set to estimate the cost functions for bifurcation and bridge forms. The resulting system has good performance in locating and correctly configuring junctions. The information that can be extracted from separate vessel segments is limited; joining these segments provides an opportunity to extract more information, and to calculate features that have never been calculated automatically before. Transforming the vascular network to a vascular graph gives researchers additional tools to analyse and understand the vascular system. The joining algorithm can efficiently join vessel segments to form a vessel graph; it could further be used in variety of vision applications, such as analysis of road junctions captured through aerial or satellite imagery.

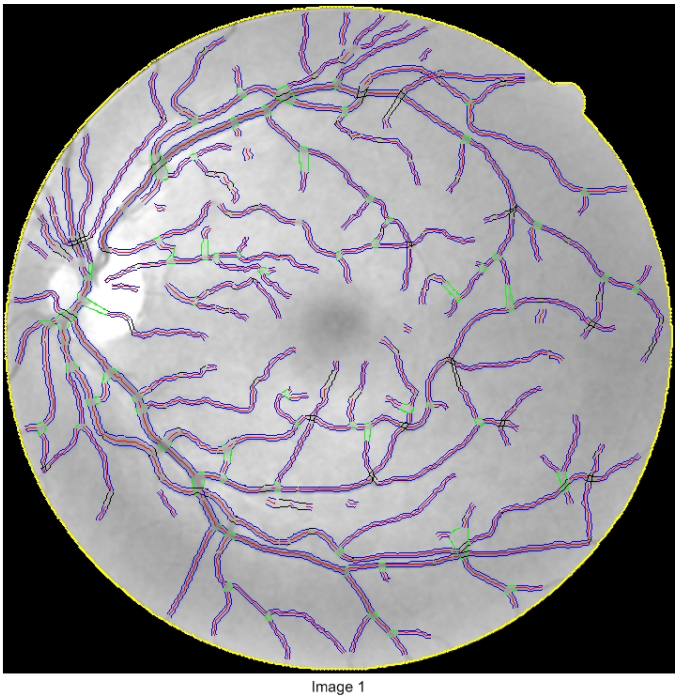

Fig. 8. The vascular graph of the first retinal image in the DRIVE database [7] is illustrated overlaid on its retinal image.

REFERENCES

[1] X. Gao, A. Bharath, A. Stanton, A. Hughes, N. Chapman, and S. Thom., "A method of vessel tracking for vessel diameter measurement on retinal images," *In Proceedings IEEE International Conference on Image Processing*, vol. 2, pp. 881–884, October 2001.

[2] M. Niemeijer, J. Staal, B. V. Ginneken, M. Loog, and M. D. Abramoff, "Comparative study of retinal vessel segmentation methods on a new publicly available database," *SPIE Medical Imaging*, vol. 5370, pp. 648–656, May 2004, j. Michael Fitzpatrick, M. Sonka.

[3] L. Gang, O. Chutatape, and S. M. Krishnan, "Detection and measurement of retinal vessels in fundus images using amplitude modified second-order gaussian filter," *IEEE Transactions on Biomedical Engineering*, vol. 49, no. 2, pp. 168–172, 2002.

[4] A. Hunter, J. A. Lowell, D. Steel, A. Basu, and R. Ryder, "Non-linear filtering for vascular segmentation and detection of venous beading," *Technical Report*, 2003.
[5] S.Aldington, E.Kohner, S.Meuer, R.Klein, A.Sjolie, and T. E. I. C. S. Group, "Methodology for retinal photography and assessment of diabetic retinopathy: the eurodiab iddm complications study," *Diabetologia*, vol. 38, no. 4, pp. 437–444, April 1995.
[6] B. Al-Diri and A. Hunter, "A ribbon of twins for extracting vessel boundaries," *The 3rd European Medical and Biological Engineering Conference EMBEC'05*, 2005.
[7] DRIVE, "Digital retinal images for vessel extraction," 2007.
[8] T. Kohonen, *Self-Organizing Maps*, 3rd ed., ser. Information Sciences. New York: Springer-Verlag, 2001.